

Design, synthesis, biological evaluation and molecular dynamics studies of 4-thiazolinone derivatives as Protein tyrosine phosphatase 1B (PTP1B) inhibitors

Wen-Shan Liu, Rui-Rui Wang, Hai Yue, Zhi-Hui Zheng, Xin-Hua Lu, Shu-Qing Wang, Wei-Li Dong & Run-Ling Wang

To cite this article: Wen-Shan Liu, Rui-Rui Wang, Hai Yue, Zhi-Hui Zheng, Xin-Hua Lu, Shu-Qing Wang, Wei-Li Dong & Run-Ling Wang (2019): Design, synthesis, biological evaluation and molecular dynamics studies of 4-thiazolinone derivatives as Protein tyrosine phosphatase 1B (PTP1B) inhibitors, Journal of Biomolecular Structure and Dynamics, DOI: [10.1080/07391102.2019.1664333](https://doi.org/10.1080/07391102.2019.1664333)

To link to this article: <https://doi.org/10.1080/07391102.2019.1664333>

 View supplementary material 

 Accepted author version posted online: 06 Sep 2019.

 Submit your article to this journal 

 View related articles 

 View Crossmark data 

Design, synthesis, biological evaluation and molecular dynamics studies of 4-thiazolinone derivatives as Protein tyrosine phosphatase 1B (PTP1B) inhibitors

Wen-Shan Liu^{a, 1}, Rui-Rui Wang^{a, 1}, Hai Yue^b, Zhi-Hui Zheng^c, Xin-Hua Lu^c, Shu-Qing Wang^a, Wei-Li Dong^{a, *}, Run-Ling Wang^{a, *}

^aTianjin Key Laboratory on Technologies Enabling Development of Clinical Therapeutics and Diagnostics (Theranostics), School of Pharmacy, Tianjin Medical University, Tianjin 300070, China.

^bInner Mongolia Institute for Drug Control, Huhhot, Inner Mongolia 010000, China.

^cNew Drug Research & Development Center of North China Pharmaceutical Group Corporation, National Microbial Medicine Engineering & Research Center, Hebei Industry Microbial Metabolic Engineering & Technology Research Center, Key Laboratory for New Drug Screening Technology of Shijiazhuang City, Shijiazhuang 050015, Hebei, China.

¹These authors contributed equally to this work.

*Correspondence to: Wei-Li Dong Email: dongweili@tmu.edu.cn

Run-Ling Wang Email: wangrunling@tmu.edu.cn

Funding information

Contract grant sponsor: National Natural Science Foundation of China; Contract grant number: 81773569.

Contract grant sponsor: National Natural Science Foundation of China; Contract grant number: 21772146.

Contract grant sponsor: Natural Science Foundation of Tianjin; Contract grant number: 18JCYBJC89800.

Abstract

Protein tyrosine phosphatase 1B (PTP1B) is a key negative regulator of insulin signaling pathway, and more and more studies have shown that it is a potential target for the treatment of type 2 diabetes mellitus (T2DM). In this study, 17 new 4-thiazolinone derivatives were designed and synthesized as novel PTP1B inhibitors, and ADMET prediction confirmed that these compounds were to be drug-like. *In vitro* enzyme activity experiments were performed on these compounds, and it was found that a plurality of compounds had good inhibitory activity and high selectivity against PTP1B protein. Among them, compound 7p exhibited the best inhibitory activity with an IC_{50} of 0.92 μ M. The binding mode of compound 7p and PTP1B protein was explored, revealing the reason for its high efficiency. In addition, molecular dynamics simulations for the PTP1B^{WT} and PTP1B^{comp#7p} systems revealed the effects of compound 7p on PTP1B protein at the molecular level. In summary, the study reported for the first time that 4-thiazolinone derivatives as a novel PTP1B inhibitor had good inhibitory activity and selectivity for the treatment of T2DM, providing more options for the development of PTP1B inhibitors.

Key words: T2DM, PTP1B inhibitor, activity, molecular docking, molecular dynamics simulation

Abbreviations

BBB (blood-brain barrier), CDC25B (cell division cycle 25 homolog B), CYP2D6 (Cytochrome P450 2D6 binding), DCCM (dynamic cross-correlation map), DS (Discovery Studio), H bond (hydrogen bond), HIA (human intestinal absorption), LAR (leukocyte antigen-related phosphatase), MD (molecular dynamics), MEG- 2 (maternal-effect germ-cell defective 2), MM-PBSA (molecular mechanics Poisson Boltzmann surface area), PCA (principal component analysis), PDB (Protein Data Bank), pNPP (p-nitrophenyl phosphate), PPB (plasma protein binding), PTP1B (protein tyrosine phosphatase 1B), RMSD (root mean square deviation), RMSF (root mean square fluctuation), SHP-1 (src homologous phosphatase-1), SHP-2 (src homologous phosphatase-2), SPC (single-point charge), TCPTP (T cell protein tyrosine phosphatase), T2DM (Type 2 diabetes mellitus), VDW (van der Waals).

1. Introduction

Type 2 diabetes mellitus (T2DM), one of the most common chronic diseases associated with numerous complications, is characterized by insulin resistance (Sun, Zhuang, et al., 2017; Tadic & Cuspidi, 2015). In 2015, more than 415 million people worldwide have diabetes, of which T2DM affects 90-95% of the total population with diabetes, and its prevalence is estimated to exceed 10% of the global adult population by 2040 (Fernandez-Silva, Alonso-Gonzalez, Gonzalez-Perez, Gestal-Otero, & Diaz-Gravalos, 2019; Sun, Zhang, et al., 2017). Therefore, T2DM has become a serious crisis threatening human health, and it is urgent to find effective strategies to treat this disease.

Usually, the abnormality of insulin signal transduction is closely related to the pathogenesis of T2DM (X. Chen, Gan, Feng, Liu, & Zhang, 2019). Protein tyrosine phosphatase 1B (PTP1B) is a member of the non-transmembrane phosphotyrosine phosphatase family, and studies have demonstrated that PTP1B is a key negative regulator in the insulin signaling pathway. PTP1B is

widely expressed in insulin-sensitive peripheral tissues and negatively regulates insulin signal transduction by dephosphorylating IRS on tyrosine residues (Byon, Kusari, & Kusari, 1998; Cheng et al., 2002; Goldstein, Bittner-Kowalczyk, White, & Harbeck, 2000; Zabolotny et al., 2002). Studies have shown that PTP1B-knockout mice show increased insulin sensitivity, improved glucose tolerance and resistance to diet-induced obesity (Elchebly et al., 1999; Klaman et al., 2000). Therefore, PTP1B is a potential new drug target for the treatment of T2DM.

In recent years, inhibitors designed against PTP1B had emerged in an endless stream. The eriprotafib developed by American Home Products was the first drug candidate to enter Phase II clinical trials (Wang et al., 2015). ISIS-113715, an antisense inhibitor of the PTP1B gene, was the second to reach phase II clinical trials (G. Liu, 2004). Unfortunately, these inhibitors were later proven to fail. These failed cases tell us that the development of clinically relevant PTP1B inhibitors still faces significant challenges and is often plagued by its poor selectivity and unfavorable pharmacokinetics (Eldehna et al., 2019). Therefore, it is increasingly important to develop PTP1B inhibitors with high selectivity and good pharmacokinetic characteristics.

Virtual screening has proven to be a very effective method for discovering new drugs with the desired properties and structural diversity (Neves et al., 2018). In this study, the scaffold ZINC99459 was found to have a good docking score and fitting value for the PTP1B protein by virtual screening method based on docking. Subsequently, based on the scaffold ZINC99459, the De novo design of the compounds was carried out to design 17 novel 4-thiazolinone derivatives. These compounds had confirmed to be drug-like by ADMET prediction. The designed compounds were subsequently synthesized. *In vitro* enzyme activity experiments were performed on PTP1B and other phosphatases, and compound 7p as the most potent selective PTP1B inhibitor was identified. Furthermore, the binding mode of the compound 7p and PTP1B protein was investigated. The conformation difference of PTP1B protein after binding with compound 7p was further explored at the molecular level by molecular dynamics (MD) simulation. Specifically, 300 ns molecular dynamics simulations were performed on the protein-ligand complex (PTP1B^{comp#7P}) and protein system (PTP1B^{WT}), respectively. A series of post-dynamics analyses were then explored the conformational differences between the two systems, including root mean square deviation (RMSD), root mean square fluctuation (RMSF), principal component analysis (PCA), and dynamic cross-correlation mapping (DCCM). In conclusion, the 4-thiazolinone derivatives were investigated as PTP1B selective inhibitors, and it was hoped to provide more clues for the development of more efficient PTP1B inhibitors.

2. Materials and methods

2.1. Compound design

2.1.1. Virtual screening based on molecular docking

Virtual screening was a very effective method for developing new drugs with the required characteristics and structural diversity (Jiang et al., 2019; Neves et al., 2018). In this study, virtual screening based on molecular docking was used for drug design by Discovery Studio (DS) 3.5 software. Firstly, the crystal structure of PTP1B protein (PDB ID: 2VEY) with the catalytic domain was downloaded from the protein data bank (PDB) and used as the receptor protein (Douty et al., 2008). The ligands for docking were retrieved from the ZINC database. Then, "Prepare

Ligands and Prepare Protein" modules were implemented for protein and ligand preparation. The binding pocket was then defined by the "Define and Edit Binding Site" tool, which produced a sphere around the receptor protein's own ligand. Finally, the retrieved ligands were docked into the receptor protein. Ligand with higher CDOKER score and fitted value was selected for further De nova design.

2.1.2. De Novo Design

Ludi was a widely used re-designed algorithm for developing new potential candidate compounds(Bohm, 1992). In our study, the De novo design method(Schneider & Fechner, 2005) was used to design new inhibitors by means of the Ludi algorithm. Firstly, the "De novo library generation protocol" was used to generate the fragment library for the De novo design. Secondly, the "De novo receptor protocol" in Discovery Studio v3.5 was used to define the binding pocket of the receptor. Based on the scaffold structure, new derivatives were developed in the binding pocket of the receptor. Finally, through the Ludi algorithm, the appropriate fragments were fitted to the scaffold obtained by virtual screening, producing a set of new derivatives with higher scores.

2.2. *In silico* ADMET prediction

The ADMET (absorption, distribution, metabolism, excretion, and toxicity) studies were performed using DS v3.5 software to assess the pharmacokinetic properties of the compounds. Some important ADMET descriptors include human intestinal absorption (HIA)(Miyake et al., 2017), blood-brain barrier (BBB)(Egan, Walters, & Murcko, 2002), plasma protein binding (PPB)(Wesson & Eisenberg, 1992), aqueous solubility(Cheng & Merz, 2003), Cytochrome P450 2D6 binding (CYP2D6)(Susnow & Dixon, 2003) and toxicity.

2.3. Chemistry

Reagents and solvents were obtained from commercial suppliers and could be used directly without further purification. Analytical thin layer chromatography (TLC) was performed on the TLC plate (silica gel 60 F254 and aluminum foil). All compounds were detected by using UV light (wavelength: 254 nm or 365 nm). The Isolation and purification of compound was carried out by flash column chromatography on silica gel 60 (300-400 mesh). ¹H (400 MHz) and ¹³C NMR (100 MHz) spectra were recorded in CDCl₃ or DMSO-*d*₆ by the spectrometer at room temperature. Chemical shifts were reported in parts per million (ppm) and coupling constants (*J*) were expressed in Hz. The characteristics of the signal were s (singlet), d (doublet), dd (doublet of doublets), t (triplet) and m (multiplet). Mass spectra were measured on an Agilent 1100 series.

2.4. *In vitro* phosphatase activity assay

Human recombinant PTP1B, SHP2, SHP1, LAR, TCPTP, MEG-2 or CDC25B was expressed in *E. coli* and purified by Ni-NTA affinity chromatography in our laboratory. The enzyme activity was measured using p-nitrophenyl phosphate (pNPP) as substrate in a 96-well plate. Briefly, purified recombinant PTP1B or other Phosphatases (0.05 µg) in 50 µl buffer containing 50mM citrate (pH 6.0), 0.1M NaCl, 1mM Ethylenediaminetetraacetic acid (EDTA), and 1mM dithiothreitol (DTT) and test compounds were added to each well of a 96-well plate. After preincubation for 15 minutes at room temperature, 50 µl of reaction buffer containing 2mM pNPP was added and incubated at

37°C for 30 min. The enzyme activity was measured by detecting the absorbance at 405 nm for the amount of produced p-nitrophenol.

2.5. Protein and ligand preparation

The crystal structure of the PTP1B protein was obtained from the Protein Data Bank (PDB) with entries 2VEY. In order to optimize the initial structure, DS v3.5 software package was used to repair the missing residues of PTP1B protein by the protocol of "Fill loops". The repaired PTP1B protein was then prepared by the Prepare Protein module, including removing water, assigning bond order, adding the hydrogen atoms, treat metals and disulfides. In addition, the structure of compound 7p was obtained by ChemDraw 8.0 and converted into MOL2 formation by Chem 3D. Subsequently, compound 7p was prepared by the "prepare ligand" module of DS v3.5, including keeping ionization, desalt and generating tautomer.

2.6. Molecular docking

Molecular docking study was performed by using the DS 3.5 software. Firstly, the preparation of proteins and the energy of the ligands was minimized by the CHARMM force field (Zhai et al., 2019). Subsequently, the receptor binding pocket was defined by the coordinate space of the extracted co-crystallized ligand (Jin, Ma, Li, Li, & Wang, 2018; Zhang, Luan, Chou, & Johnson, 2002). The binding pocket of a protein was generally defined by a residue having at least one heavy atom, and the distance between this heavy atom and the heavy atom of the ligand was 5 Å (Ma, Wang, Xu, Wang, & Chou, 2012). Finally, the docking module in the DS v3.5 program was performed to dock the ligands into the protein. The conformation with the highest docking score was used to analyze the interaction between the protein and the ligand.

2.7. Molecular Dynamics Simulation

MD simulations for PTP1B^{WT} and PTP1B^{comp#7p} systems were performed using the GROMACS 4.5.5 software package with CHAMM27 force field (Pol-Fachin, Fernandes, & Verli, 2009). First, a file called "topology" was generated that contained simulation information about the nonbonding parameters (atom types and charges) and the bonding parameters (bonds, angles and dihedrals). Then, the system was simulated by incorporating space-filling dodecahedron boxes and filled with explicit single-point charge (SPC) water molecules (the number of water molecules was 3400). The distance from the surface of the protein to the edge of the box was limited to at least 1 nm and the system is neutralized by adding 6 sodium ions. Subsequently, the steepest descent method was used to ensure that there were no steric clash and inappropriate geometry in the system, and the energy of the system was minimized to 1000 kJ·mol⁻¹ / nm (Tang et al., 2018). At the same time, the system got a better balance by the 100 ps position restrained equilibration dynamics simulation, namely NVT and NPT canonical ensemble. Where, N was part number, P was system pressure, V was volume, and T was temperature. During the NVT simulation, the system was heated from 0 to 300 K with the thermostat and stabilized at 300 K. During the NPT simulation, the system pressure was maintained at 1 bar by using a constant pressure device. In addition, all hydrogen-bonded atoms in the system were suitable for the LINCS algorithm (Hess, 2008). Finally, 300 ns MD simulation was performed.

2.8. Principal Component Analysis (PCA)

PCA was a statistical technique that has been widely used to understand the conformational differences of protein system (Balmith & Soliman, 2017). This method was based on building a covariance matrix of complex sets of variables and was used to reduce the dimensionality of the data to gain valuable information from the protein system throughout the molecular dynamics simulation (Maisuradze, Liwo, & Scheraga, 2009; Yesudhas et al., 2016). The ensemble formula used to calculate the covariance matrix C_{ij} for each pair of $C\alpha$ atoms i and j was based on the following equation (Zhou, Zhang, Chen, Zhao, & Zhong, 2016):

$$C_{ij} = \langle (x_i - \langle x_i \rangle) (x_j - \langle x_j \rangle) \rangle \quad (i, j = 1, 2, 3, \dots, N)$$

Here, x_i and x_j were the i th and j th Cartesian coordinates of $C\alpha$ atoms, respectively. $\langle x_i \rangle$ and $\langle x_j \rangle$ were the time average over all the configurations gained in MD simulation, and N was the number of carbon atoms. The eigenvectors of the matrix were taken as the principal component (PC), which indicated the projections of trajectory on the principal mode. And, the corresponding eigenvalues represented the direction of PC. Usually, the first few principal components were used to describe the overall motion of the system (Fakhar et al., 2017). The PCA scatter plot was generated by Bio3d software (Grant, Rodrigues, ElSawy, McCammon, & Caves, 2006).

2.9. Dynamic Cross-Correlation Map (DCCM) Analysis

To detect the dynamic correlation among different protein domains, DCCM analysis was performed to analyze the correlation matrix across all $C\alpha$ atoms of PTP1B^{WT} system and PTP1B^{comp#7p} system (Xu, Kong, Zhu, Sun, & Chang, 2016). Cross-correlation coefficient C_{ij} for the pair of each $C\alpha$ atoms i and j was calculated the following equation (Ndagi, Mhlongo, & Soliman, 2017):

$$C_{ij} = \langle \Delta r_i \cdot \Delta r_j \rangle / \{ \langle \Delta r_i^2 \rangle \langle \Delta r_j^2 \rangle \}^{1/2}$$

Here, Δr_i (Δr_j) represented the displacement vector of the i th (j th) atom of the systems, and i and j represented the i -th and j -th atom, and $\langle \dots \rangle$ indicated ensemble average. The value of C_{ij} was from -1 to 1. Positive values indicated positively correlated movement (the same direction), and negative values indicated anti-correlated movement (the opposite direction) (Li et al., 2014). The higher the absolute value of C_{ij} , the greater the correlation (or inverse correlation) between the two residues (Olde Scheper, Meredith, Mansvelder, van Pelt, & van Ooyen, 2017).

3. Results and discussion

3.1. Compound design

The scaffold ZINC99459 (Figure 1) was found by virtual screening with a higher docking score and fitted value. The searched fragments were fitted to the scaffold ZINC99459 by the De nova design method, and a series of new compounds 7a-q were obtained based on the docking scores and fitted value.

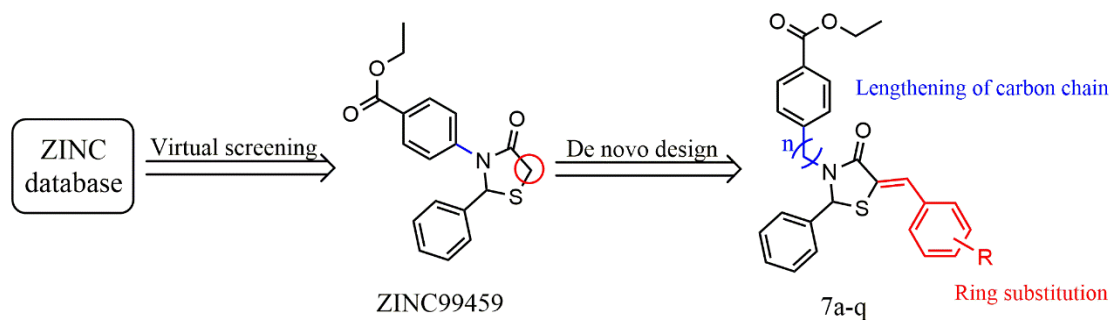


Figure 1. Design strategy of the target compounds.

3.2. *In silico* ADMET prediction

ADMET prediction was considered a key step for drug candidates (Thiyagarajan, Lin, Chang, & Weng, 2016). The ADMET properties of all design compounds 7a-q were predicted and compared by using DS v3.5. For the aqueous solubility level: 0 (extremely low); 1 (very low, but possible), 2 (low), 3 (good); for the PPB level: 0 meant that the binding level was below 90%, 1 meant that the binding level was above 90%, and 2 meant that the binding level was above 95%; for the BBB level: 0 (very good), 1 (good), 2 (moderate), 3 (poor), 4 (undefined); for the CYP2D6 Probability level: Less than 0.5 meant that it was unlikely to inhibit CYP2D6 (Non-CYP2D6 inhibitors), and above 0.5 meant that it was likely to inhibit CYP2D6 enzyme (CYP2D6 Inhibitors); for the hepatotoxic prediction, true represented non-hepatotoxic and for HIA level: 0 (good), 1 (moderate), 2 (poor), 3 (very poor). The ADMET prediction results of these compounds were listed in Tables S1 and S2. According to the predicted results, these 17 compounds were confirmed to be drug-like and had low side effects.

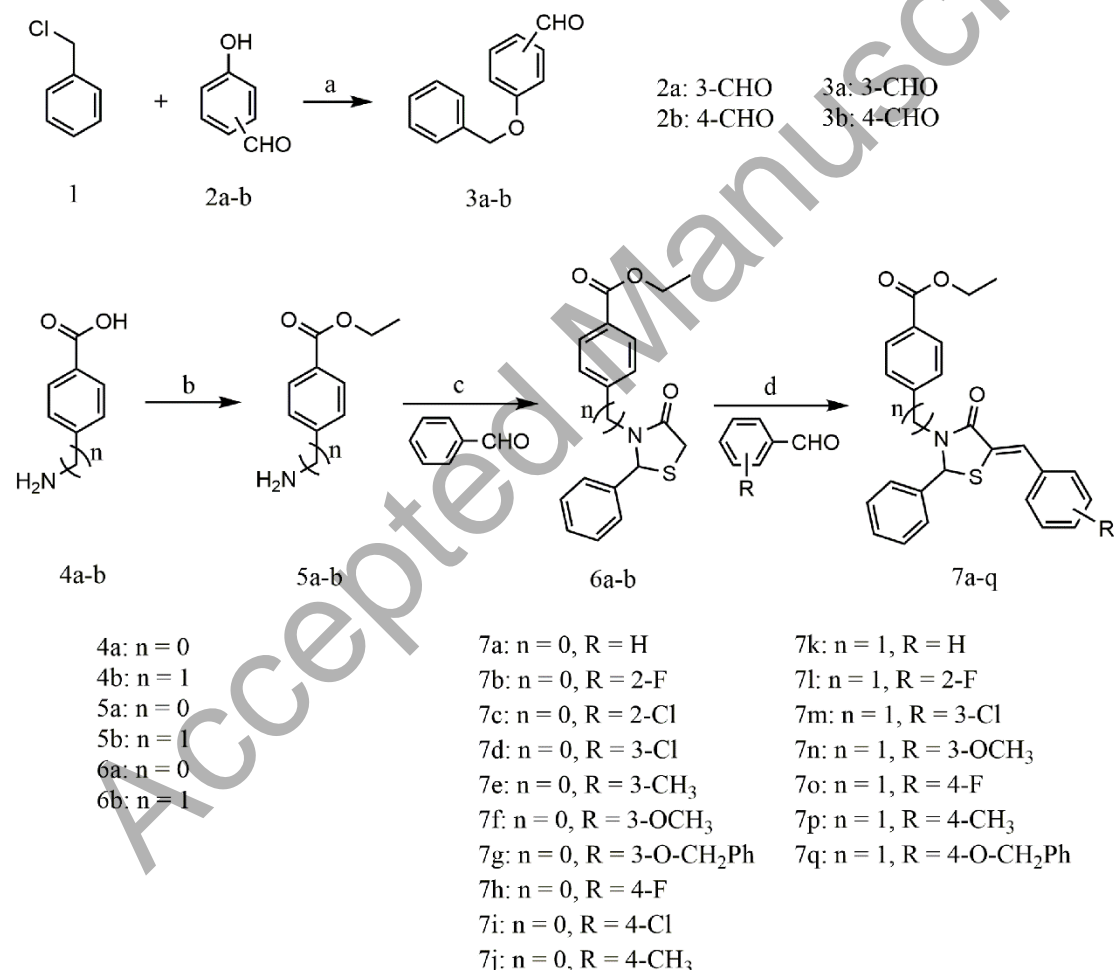
3.3. Chemistry

A mixture of benzyl chloride (1) (30 mmol), hydroxybenzaldehyde derivatives 2a-b (40 mmol), and anhydrous potassium carbonate (K_2CO_3) (90 mmol) in N,N-Dimethylformamide (DMF) (80 mL). The completion of the reaction was detected by TLC analysis. The mixture was extracted with ethyl acetate (EtOAc) (3×60 mL) and washed with 5% brine solution (3×60 mL). The combined organic layers were dried with anhydrous sodium sulphate ($NaSO_4$). The obtained residue was purified by silica gel column chromatography (PE : EA = 4 : 1) to afford Intermediate 2a-i.

The p-aminobenzoic acid derivatives 4a-b (50 mmol) was added to absolute ethanol (EtOH) (100 mL) to form a white suspension. Under ice bath conditions, thionyl chloride (175 mmol) was slowly added dropwise to the suspension. After the dropwise addition was completed, the suspension was stirred at room temperature for 30 min, and then heated to reflux for 4 h. After completion of the reaction, the volatile solvent was concentrated under reduced pressure to obtain white solid. The solid was dissolved in EtOAc (150 mL) to obtain a white suspension. Under ice bath, 25% Sodium hydroxide (NaOH) aqueous solution (60 mL) was slowly added and stirred for 30 min. The white suspension gradually became clear solution with pH of from 7 to 8. After standing, the aqueous layer was removed, and the organic layer was washed with saturated salt solution (30×60 mL), and dried over anhydrous $NaSO_4$. The solvent was removed under reduced pressure to obtain intermediates 5a-b.

The ethyl p-aminobenzoate derivatives 5a-b (50 mmol) were dissolved in tetrahydrofuran (THF)

(300 mL) and benzaldehyde (100 mmol) and dicyclohexylcarbodiimide (DCC) (60 mmol). Mercapto acetic acid (100 mmol) was slowly added dropwise to the mixture under ice bath. After the dropwise addition was completed, the reaction was stirred at room temperature for 3 h. After the reaction was completed, the white solid in the mixture was removed by filtration. The volatile solvent was then removed under reduced pressure to obtain white solid. EtOAc (350 mL) was added to white solid to dissolve, and then the organic layer was washed successively with 5% citric acid aqueous solution (3×70 mL), distilled water (3×70 mL), 5% sodium bicarbonate (NaHCO_3) aqueous sodium (3×70 mL) and saturated aqueous sodium chloride solution (3×70 mL). Finally, the white solid was recrystallized from absolute EtOH to obtain intermediates 6a-b. Sodium metal (4 mmol) was cut into small sodium particles and added to absolute EtOH (20 mL) to form an alcohol solution of sodium ethoxide (EtONa). Intermediates 6a-b (4 mmol) and benzaldehyde derivatives (4 mmol) were added to absolute EtOH (30 mL) and stirred to dissolve completely. Then, alcohol solution of EtONa was slowly added dropwise, and the mixture was heated under reflux for 30 min. After completion of the reaction, the solvent was evaporated under reduced pressure, and the residue obtained was purified by silica gel chromatography on silica gel (PE : EA = 5 : 1) to obtain the final products 7a-q.



Scheme 1. Synthetic scheme for the synthesis of compounds 7a-q. Reagents and conditions: (a) K_2CO_3 , DMF, 55°C , 3 h; (b) SOCl_2 , EtOH, $0^\circ\text{C} \sim 80^\circ\text{C}$, 4.5h; (c) Mercapto acetic acid, DCC, THF, $0^\circ\text{C} \sim \text{rt}$, 4 h; (d) Sodium, EtOH, 80°C , 0.5 h.

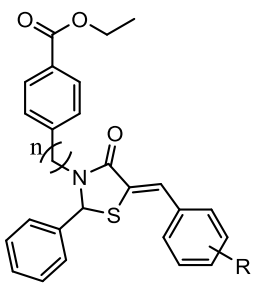
3.4. Biological evaluation

Table 1 listed the inhibitory activities of 17 4-thiazolinone derivatives against PTP1B and other phosphatases. It could be seen from the table that multiple compounds exhibited good inhibitory activity against PTP1B protein with IC_{50} values ranging from 0.92 to 9.64 μM . Among them, compound 7p showed the most potent inhibitory activity with an IC_{50} value of 0.92 μM . Subsequently, study of the structure-activity relationship (SAR) was carried out.

When $n = 0$, different R substituents had large effects on the inhibitory activity. Specifically, when there was no substitution on the substituent R, the compound 7a exhibited an inhibitory activity with an IC_{50} of 3.23 μM . When the substituent R was a 2-position substitution, the activity of the 2-position Cl substitution (7c, $IC_{50} = 4.02 \mu\text{M}$) was significantly higher than that of the 2-position F substitution (7b, $IC_{50} = 9.64 \mu\text{M}$). When the substituent R was a 3-position substitution, the activity of the 3-position CH_3 substitution (7e, $IC_{50} = 2.09 \mu\text{M}$) was significantly higher than that of the other 3-position substituents (7d, 7f and 7g). When the substituent R was a 4-position substitution, the activity of the 4-position CH_3 substitution (7g, $IC_{50} = 1.39 \mu\text{M}$) was significantly higher than that of the other 4-position substituents (7h and 7i). Moreover, the activity of the 4-position CH_3 substitution was higher than that of the 3-position CH_3 substitution (7g vs 7e), indicating that the 4-position CH_3 substitution was a dominant substituent. When $n = 1$, its SAR was similar to that of $n = 0$. It was found that the activity of the 4-position CH_3 substitution (7p, $IC_{50} = 0.92 \mu\text{M}$) was significantly higher than that of the other substituents. Furthermore, by comparing the values of n , it was found that the introduction of CH_2 ($n = 1$) in the structure could significantly increase the inhibitory activity (7p vs 7g) with a 1.5-fold increase in activity.

As shown in Table 1, we also explored the selectivity of these 17 compounds for other phosphatases, including homogeneous T cell protein tyrosine phosphatase (TCPTP), src homologous phosphatase-2 (SHP-2), src homologous phosphatase-1 (SHP-1), cell division cycle 25 homolog B (CDC25B), leukocyte antigen-related phosphatase (LAR) and maternal-effect germ-cell defective 2 (MEG-2). We had focused on the selectivity of compounds 7e, 7g, 7m and 7p with good inhibitory activity against other phosphatases. It could be seen from the table that these four compounds showed more than 15-fold greater selectivity for PTP1B than for TCPTP, more than 12-fold selectivity for PTP1B over SHP-1, more than 18-fold selectivity for PTP1B over CDC25B, and more than 10-fold selectivity for PTP1B over MEG-2. In addition, these four compounds had almost no activity on SHP-2 and LAR, both with IC_{50} values over 100 μM . In short, after our efforts, we had developed multiple compounds that had good inhibitory activity and high selectivity for PTP1B protein.

Table 1. Inhibitory activity of compound 7a-q on PTP1B and other phosphatases.

 7a-p									
Compd.	n	R	PTP1B IC ₅₀ (μ M)	TCPTP IC ₅₀ (μ M)	SHP2 IC ₅₀ (μ M)	SHP1 IC ₅₀ (μ M)	CDC25 B IC ₅₀ (μ M)	LAR IC ₅₀ (μ M)	MEG-2 IC ₅₀ (μ M)
ZINC-9 9459	-	-	50.24	NA	NA	NA	NA	NA	NA
7a	0	H	3.23	>100	>100	3.60	>100	>100	4.16
7b	0	2-F	9.64	>100	>100	3.08	>100	>100	4.34
7c	0	2-Cl	4.02	9.05	>100	>100	>100	>100	>100
7d	0	3-Cl	3.97	>100	>100	>100	>100	>100	>100
7e	0	3-CH ₃	2.09	30.21	>100	>100	39.03	>100	>100
7f	0	3-OCH ₃	4.05	13.20	>100	>100	>100	>100	>100
7g	0	3-OCH ₂ Ph	2.88	8.63	0.96	>100	>100	>100	>100
7h	0	4-F	7.51	>100	>100	4.74	>100	>100	6.87
7i	0	4-Cl	4.89	>100	>100	2.97	>100	>100	12.92
7j	0	4-CH ₃	1.39	>100	>100	16.69	>100	>100	14.85
7k	1	H	3.22	24.75	>100	>100	>100	>100	>100
7l	1	2-F	8.05	>100	>100	2.71	>100	>100	6.03
7m	1	3-Cl	2.40	>100	>100	>100	>100	>100	>100
7n	1	3-OCH ₃	3.03	29.31	>100	>100	>100	>100	>100
7o	1	4-F	6.26	>100	62.85	2.53	>100	>100	32.35
7p	1	4-CH ₃	0.92	>100	>100	22.23	>100	>100	>100
7q	1	4-OCH ₂ Ph	5.61	>100	>100	1.14	>100	>100	>100

The "NA" indicated that the compound was not tested.

3.5. Study of the binding mode

Molecular docking was used to simulate the binding mode between compound 7p and PTP1B protein and to understand their interactions in depth (J. Liu, Wang, Ma, Wang, & Wang, 2011). The PTP1B protein had two binding sites: a catalytically active site (CYS215-ARG221) and a second aromatic binding site (ARG24, ARG254, MET258, GLY259, GLN262 and GLN266) (Y. Y. Chen et al., 2008). As shown in Figure 2A, compound 7p with a higher inhibitory activity was well docked to the active pocket of PTP1B with the help of DS 3.5 software. The top-ranked docking score for compound 7p and PTP1B protein was 45.1248. As shown in Figure 2B, the interaction of compound 7p and PTP1B was clearly shown. Among them, the compound 7p formed hydrogen

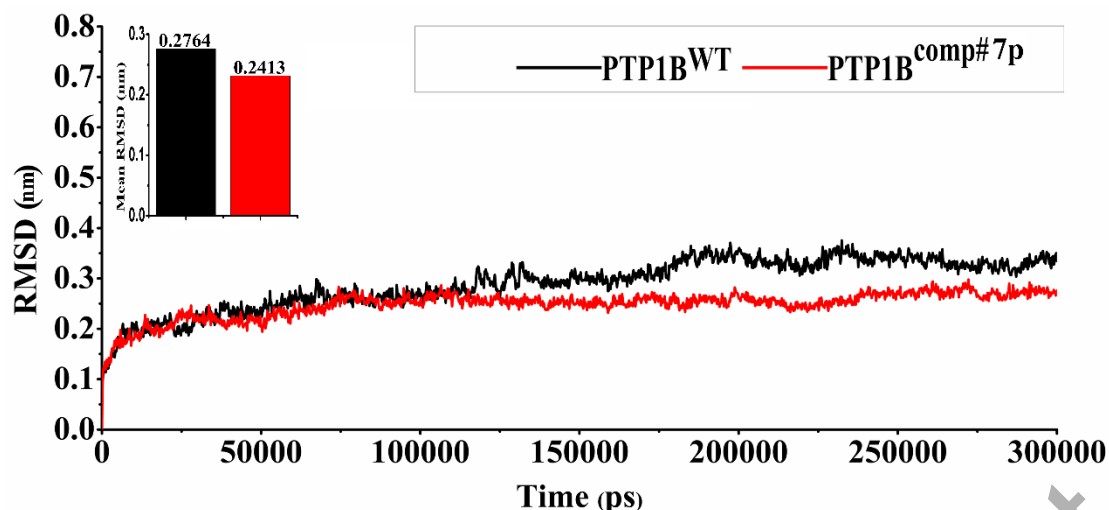


Figure 3. RMSD of all backbone atoms of two systems. The black line represents the RMSD of the PTP1B^{WT} system. The red line means the RMSD of the PTP1B^{comp#7p} system. The average values of RMSD are represented as bar graph of the upper left corner.

3.6.2. Evaluation on the flexibility of side chain residues

Residues were component of protein that determined its conformational features. Interactions such ligand-residue interaction in the active site might induce conformational changes in protein structure and alter its function (J. Chen, Wang, Pang, Zhang, & Zhu, 2019). More specifically, the conformational changes occur as a result of ligand-induced motion during ligand binding (Loeffler & Winn, 2013). Understanding ligand-induced conformational changes in the protein structure are critical to structure-based rational drug design. RMSF was a measure of average atomic mobility of backbone atoms (N, C α , and C) during MD simulations (Ndagi, Mhlongo, & Soliman, 2018). To understand and explore the structural dynamics that took place upon the ligand binding, RMSF of the subject systems was calculated from the 300 ns MD trajectories and the plot is presented in Figure 4. It was reflected that the flexibility of most residues in the PTP1B^{WT} system was similar to that in the PTP1B^{comp#7p} system. The greater the value of RMSF, the greater the flexibility of residues. The differences in flexibility were observed in the catalytic active region (residues CYS215-ARG221). Similarly, the region (residues ARG254-GLN266) also exhibited higher fluctuations in the PTP1B^{WT} system. The RMSF values of the residues CYS215-ARG221 and ARG254-GLN266 in the PTP1B^{WT} were 0.11 nm and 0.09 nm higher than that in PTP1B^{comp#7p}, respectively. Obviously, the compound 7p had reduced the flexibility in regions (CYS215-ARG221 and ARG254-GLN266), which might lead to the decrease in the catalytic activity of the PTP1B protein.

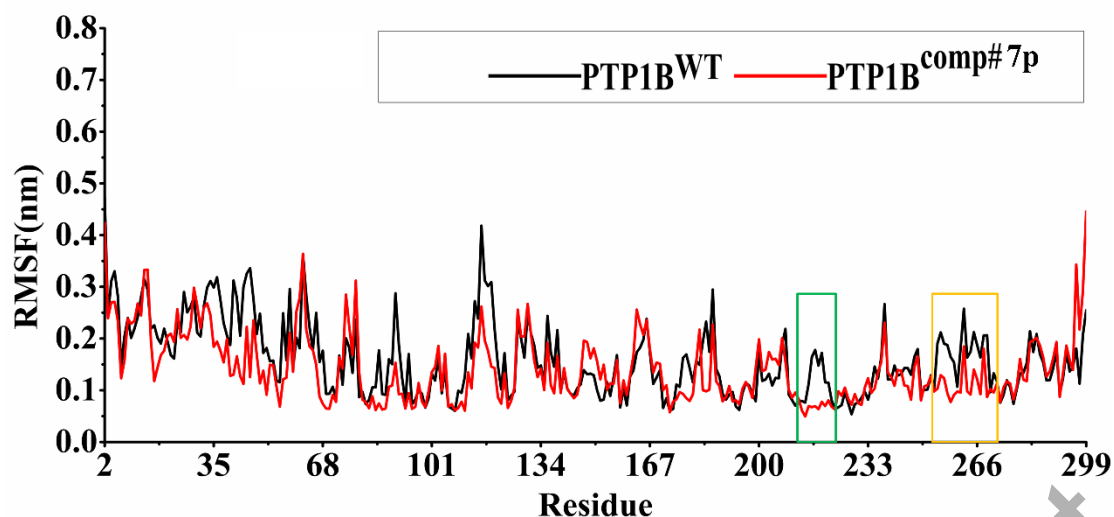


Figure 4. The RMSF of the side- chain atoms for PTP1B^{WT} system and PTP1B^{comp#7p} system. The red line indicates the outcome for the PTP1B^{comp#7p} system and the black line represents the outcome for the PTP1B^{WT} system. Meanwhile, the region (residues CYS215-ARG221) and region (residues ARG254-GLN266) are highlighted by the green frame and yellow frame, respectively.

3.6.3. The analysis for the conformational states of the two systems

In order to explore the conformational state of the two proteins during the MD simulation, PCA was performed on all C α atoms in the PC phase space. The conformational behavior of the PTP1B^{WT} system and the PTP1B^{comp#7p} system was obtained by projecting their trajectories into a two-dimensional subspace spanning along first major PCs (PC1 and PC2) (W. S. Liu, Wang, Sun, et al., 2019). From the Figure 5, the first two eigenvectors (PC1 and PC2) that occupied most of the variance in the original distribution of the protein conformation space could be used to analyze the conformational state of the two systems. PCA scatter plot showed two kinds of conformational states in subspace. Blue dots represented unstable conformational states, red dots represented stable conformational states, and white dots represent intermediate states between two conformations. The protein system periodically switched between two conformational states (blue and red) (W. S. Liu, Wang, Li, et al., 2019). From PCA results, it could be seen that the conformational state of proteins had changed significantly between the two systems. Compared with PTP1B^{WT} system (Figure 5A), the conformational state of PTP1B^{comp#7p} system (Figure 5B) was more concentrated, suggesting that the existence of ligands restricted the movement of proteins. From the 11-300 ns simulation trajectories, the top 20 PCs in the PTP1B^{WT} system and PTP1B^{comp#7p} system occupied 73% and 80.9% of the total variation, respectively. In PTP1B^{WT} system, the contributions of the first two PCs (PC1 and PC2) to the variance were 31.0% and 11.6%, respectively. In PTP1B^{comp#7p} system, the contributions of the first two PCs to the variance were 38.2% and 15.0%, respectively. It could be seen that PTP1B^{comp#7p} system occupied smaller phase space and exhibited lower flexibility than PTP1B^{WT} system.

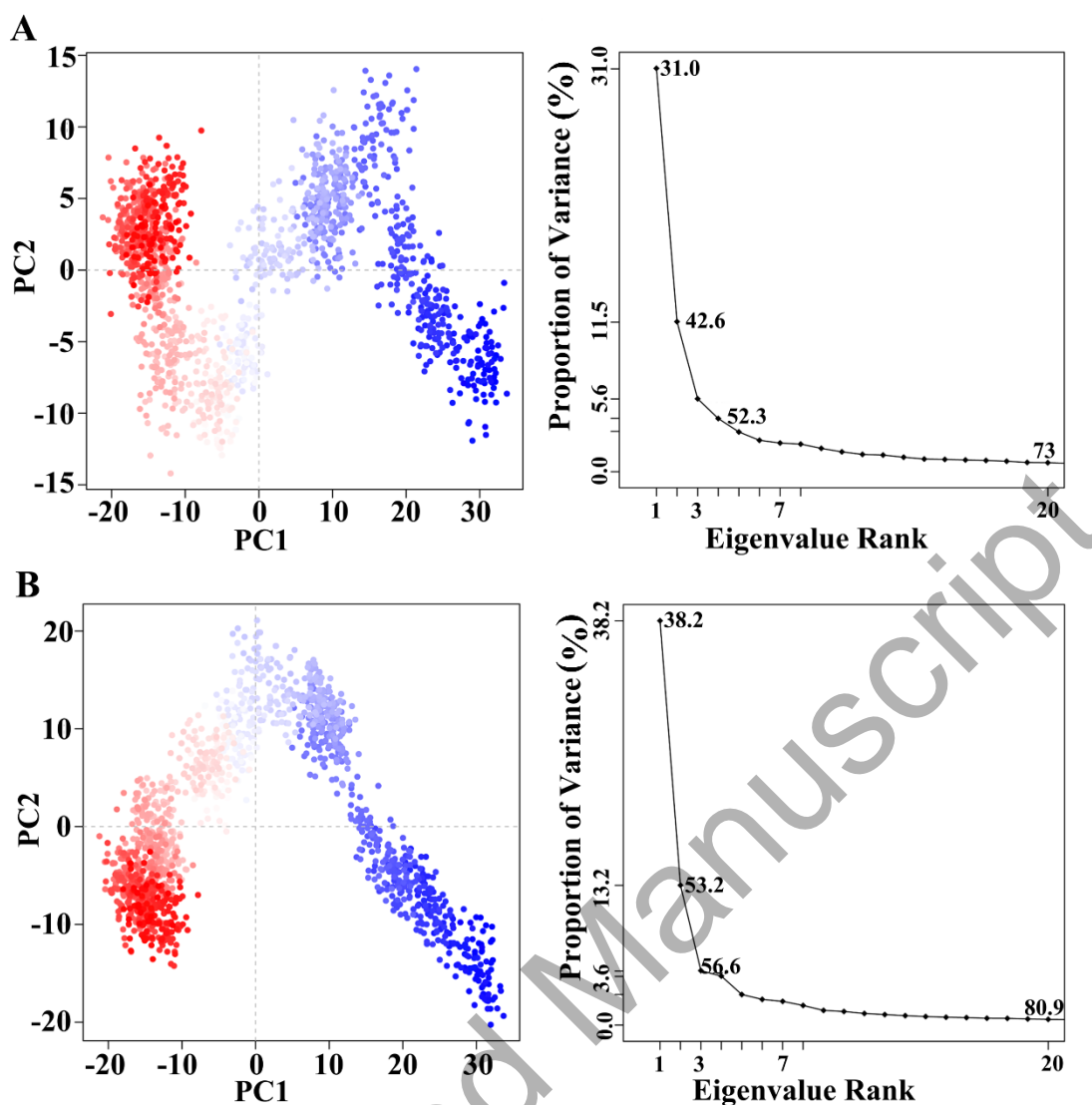


Figure 5. Projections of trajectories onto the first two principal components (PC1 and PC2) in the phase space. (A) Projection for PTP1B^{WT} system. (B) Projection for PTP1B^{comp#7p} system. Different conformational states are represented by two different color points, here, red represents the stable conformational state and blue represents the unstable conformational state.

3.6.4. The analysis for the correlated motions of the two systems

Dynamic cross-correlation map (DCCM) showed the overall landscape of the correlated motion between residues during MD simulation (Ndagi et al., 2017). To investigate the difference in correlated motion between PTP1B^{WT} system and PTP1B^{comp#7p} system, the DCCM of all C α atoms during the entire simulations was analyzed (Yan et al., 2019). The correlated motions of the C α atoms from the 11-300 ns simulated trajectories of two systems were displayed in Figure 6. The different colors represented the different correlations. The strong negative correlated motions of the residues ranged from 0 to -1 (from white to light blue to dark blue), and conversely, strong positive correlated motions of the residues ranged from 0 to 1 (from white to light red to dark red) (Machaba, Mhlongo, & Soliman, 2018). The darker the areas, the stronger the correlation between the residues. By analyzing the DCCM, the correlated motions between the regions of the PTP1B protein was significantly altered due to the binding of the compound 7p. It was found that

the overall correlated motion of residues in the PTP1B^{comp#7p} system was significantly reduced compared to the PTP1B^{WT} system. For better observation, the regions with significant differences in the correlated motion were highlighted by the black frames. In PTP1B^{WT} system, the catalytic active region (residues CYS215–AYS221) and regions (residues GLU8–TYR46 and PRO180–PRO210) showed highly positive correlation. However, in PTP1B^{comp#7p} system, the positive correlation between the region (residues CYS215–ARG221) and regions (residues GLU8–TYR46 and PRO180–PRO210) was significantly attenuated. Therefore, the compound 7p resulted in a significant decrease in the correlated motions of residues in the PTP1B protein, indicating that PTP1B^{comp#7p} system had a higher stability in conformation than PTP1B^{WT} system.

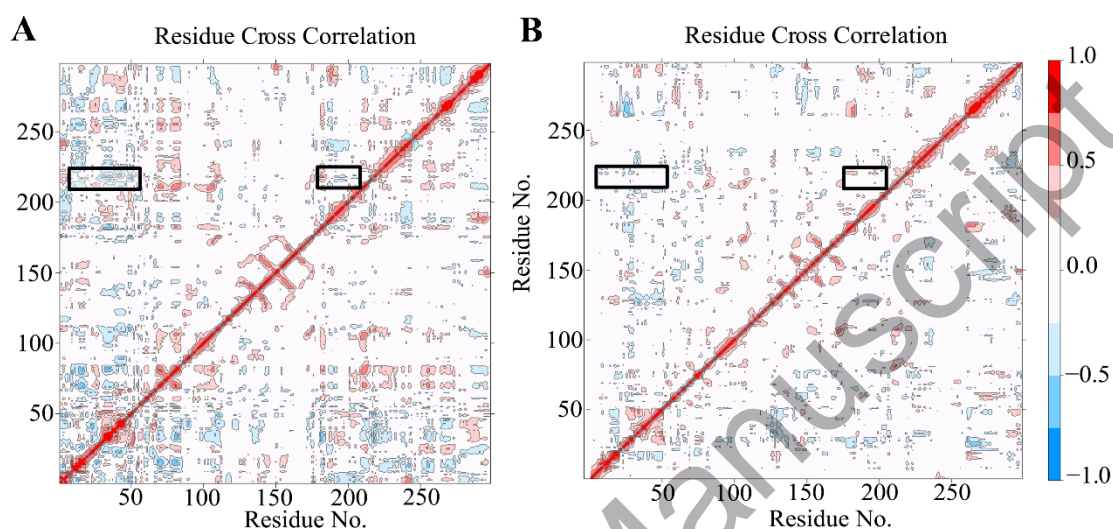


Figure 6. A, the DCCM analyses of C α atoms for PTP1B^{WT} system. B, the DCCM analyses of C α atoms for PTP1B^{comp#7p} system. Blue regions mean negative correlation while red regions mean positive correlation, and the deeper the color, the stronger the correlation. The catalytic active region is marked in black frames.

4. Conclusion

PTP1B has attracted widespread attention as a target for the treatment of T2DM. In this study, 17 4-thiazolinone derivatives were designed and synthesized as novel PTP1B inhibitors. ADMET prediction confirmed that these compounds were potential to be drug-like. *In vitro* enzyme activity experiment found multiple compounds with developmental value. Among them, compound 7p had the best inhibitory activity with an IC₅₀ of 0.92 μ M. The binding mode of compound 7p and PTP1B protein was explored by molecular docking. It was found that the stable interactions between compound 7p and PTP1B protein was formed, revealing the underlying reason why compound 7p had high inhibitory activity on PTP1B protein at the molecular level. Furthermore, 300 ns molecular dynamics simulations were performed on both PTP1B^{WT} and PTP1B^{comp#7p} systems. A series of the post-dynamics analyses were performed on the simulated trajectories of these two systems to investigate the effects of compound 7p on PTP1B protein. The stability of the two systems was evaluated by RMSD, and it was found that both systems reached steady state around 10 ns. The average RMSD value of the PTP1B^{comp#7p} system was smaller than that of the PTP1B^{WT} system, indicating that the stability of the protein after binding to the ligand was significantly enhanced. The flexibility of the two systems was evaluated by RMSF and it was

found that there were significant differences in the RMSF of the two systems at the catalytic active region (residues CYS215-ARG221) and the region (residues ARG254-GLN266). It was found that the binding of compound 7p and PTP1B protein caused significant decrease in the flexibility of these two regions. Analyses of PCA and DCCM revealed that the PTP1B^{comp#7p} system occupied a smaller phase space and the correlated motions between the residues were significantly reduced, indicating increase in protein rigidity after binding with the ligand. In summary, through this series of studies, more clues are provided for further development of more efficient selective PTP1B inhibitors.

CONFLICT OF INTEREST

The authors report no conflicts of interest in this work.

References

- Balmith, M., & Soliman, M. E. (2017). Non-active site mutations disturb the loop dynamics, dimerization, viral budding and egress of VP40 of the Ebola virus. *Mol Biosyst*, *13*(3), 585-597. doi: 10.1039/c6mb00803h
- Bohm, H. J. (1992). The computer program LUDI: a new method for the de novo design of enzyme inhibitors. *J Comput Aided Mol Des*, *6*(1), 61-78.
- Byon, J. C., Kusari, A. B., & Kusari, J. (1998). Protein-tyrosine phosphatase-1B acts as a negative regulator of insulin signal transduction. *Mol Cell Biochem*, *182*(1-2), 101-108.
- Chen, J., Wang, X., Pang, L., Zhang, J. Z. H., & Zhu, T. (2019). Effect of mutations on binding of ligands to guanine riboswitch probed by free energy perturbation and molecular dynamics simulations. *Nucleic Acids Res*, *47*(13), 6618-6631. doi: 10.1093/nar/gkz499
- Chen, X., Gan, Q., Feng, C., Liu, X., & Zhang, Q. (2019). Investigation of selective binding of inhibitors to PTP1B and TCPTP by accelerated molecular dynamics simulations. *J Biomol Struct Dyn*, *37*(14), 3697-3706. doi: 10.1080/07391102.2018.1526117

- Chen, Y. Y., Chu, H. M., Pan, K. T., Teng, C. H., Wang, D. L., Wang, A. H., . . . Meng, T. C. (2008). Cysteine S-nitrosylation protects protein-tyrosine phosphatase 1B against oxidation-induced permanent inactivation. *J Biol Chem*, *283*(50), 35265-35272. doi: 10.1074/jbc.M805287200
- Cheng, A., & Merz, K. M., Jr. (2003). Prediction of aqueous solubility of a diverse set of compounds using quantitative structure-property relationships. *J Med Chem*, *46*(17), 3572-3580. doi: 10.1021/jm020266b
- Cheng, A., Uetani, N., Simoncic, P. D., Chaubey, V. P., Lee-Loy, A., McGlade, C. J., . . . Tremblay, M. L. (2002). Attenuation of leptin action and regulation of obesity by protein tyrosine phosphatase 1B. *Dev Cell*, *2*(4), 497-503.
- Douty, B., Wayland, B., Ala, P. J., Bower, M. J., Pruitt, J., Bostrom, L., . . . Yue, E. W. (2008). Isothiazolidinone inhibitors of PTP1B containing imidazoles and imidazolines. *Bioorg Med Chem Lett*, *18*(1), 66-71. doi: 10.1016/j.bmcl.2007.11.012
- Egan, W. J., Walters, W. P., & Murcko, M. A. (2002). Guiding molecules towards drug-likeness. *Curr Opin Drug Discov Devel*, *5*(4), 540-549.
- Elchebly, M., Payette, P., Michaliszyn, E., Cromlish, W., Collins, S., Loy, A. L., . . . Kennedy, B. P. (1999). Increased insulin sensitivity and obesity resistance in mice lacking the protein tyrosine phosphatase-1B gene. *Science*, *283*(5407), 1544-1548. doi: 10.1126/science.283.5407.1544
- Eldehna, W. M., Abdelrahman, M. A., Nocentini, A., Bua, S., Al-Rashood, S. T., Hassan, G. S., . . . Supuran, C. T. (2019). Synthesis, biological evaluation and in silico studies with 4-benzylidene-2-phenyl-5(4H)-imidazolone-based benzenesulfonamides as novel

- selective carbonic anhydrase IX inhibitors endowed with anticancer activity. *Bioorg Chem*, *90*, 103102. doi: 10.1016/j.bioorg.2019.103102
- Fakhar, Z., Govender, T., Maguire, G. E. M., Lamichhane, G., Walker, R. C., Kruger, H. G., & Honarparvar, B. (2017). Differential flap dynamics in I,d-transpeptidase2 from mycobacterium tuberculosis revealed by molecular dynamics. *Mol Biosyst*, *13*(6), 1223-1234. doi: 10.1039/c7mb00110j
- Fernandez-Silva, M. J., Alonso-Gonzalez, A., Gonzalez-Perez, E., Gestal-Otero, J. J., & Diaz-Gravalos, G. J. (2019). [Health literacy in patients with type 2 diabetes: A cross-sectional study using the HLS-EU-Q47 questionnaire]. *Semergen*, *45*(1), 30-36. doi: 10.1016/j.semerg.2018.08.003
- Goldstein, B. J., Bittner-Kowalczyk, A., White, M. F., & Harbeck, M. (2000). Tyrosine dephosphorylation and deactivation of insulin receptor substrate-1 by protein-tyrosine phosphatase 1B. Possible facilitation by the formation of a ternary complex with the Grb2 adaptor protein. *J Biol Chem*, *275*(6), 4283-4289. doi: 10.1074/jbc.275.6.4283
- Grant, B. J., Rodrigues, A. P., ElSawy, K. M., McCammon, J. A., & Caves, L. S. (2006). Bio3d: an R package for the comparative analysis of protein structures. *Bioinformatics*, *22*(21), 2695-2696. doi: 10.1093/bioinformatics/btl461
- Hess, B. (2008). P-LINCS: A Parallel Linear Constraint Solver for Molecular Simulation. *J Chem Theory Comput*, *4*(1), 116-122. doi: 10.1021/ct700200b
- Jiang, C. S., Ge, Y. X., Cheng, Z. Q., Wang, Y. Y., Tao, H. R., Zhu, K., & Zhang, H. (2019). Discovery of New Selective Butyrylcholinesterase (BChE) Inhibitors with Anti-Abeta Aggregation Activity: Structure-Based Virtual Screening, Hit Optimization and

Biological Evaluation. *Molecules*, 24(14). doi: 10.3390/molecules24142568

Jin, W. Y., Ma, Y., Li, W. Y., Li, H. L., & Wang, R. L. (2018). Scaffold-based novel SHP2 allosteric inhibitors design using Receptor-Ligand pharmacophore model, virtual screening and molecular dynamics. *Comput Biol Chem*, 73, 179-188. doi: 10.1016/j.compbiolchem.2018.02.004

Klaman, L. D., Boss, O., Peroni, O. D., Kim, J. K., Martino, J. L., Zabolotny, J. M., . . . Kahn, B. B. (2000). Increased energy expenditure, decreased adiposity, and tissue-specific insulin sensitivity in protein-tyrosine phosphatase 1B-deficient mice. *Mol Cell Biol*, 20(15), 5479-5489. doi: 10.1128/mcb.20.15.5479-5489.2000

Li, X., Wang, X., Tian, Z., Zhao, H., Liang, D., Li, W., . . . Lu, S. (2014). Structural basis of valmerins as dual inhibitors of GSK3beta/CDK5. *J Mol Model*, 20(9), 2407. doi: 10.1007/s00894-014-2407-1

Liu, G. (2004). Technology evaluation: ISIS-113715, Isis. *Curr Opin Mol Ther*, 6(3), 331-336.

Liu, J., Wang, F., Ma, Z., Wang, X., & Wang, Y. (2011). Structural determination of three different series of compounds as Hsp90 inhibitors using 3D-QSAR modeling, molecular docking and molecular dynamics methods. *Int J Mol Sci*, 12(2), 946-970. doi: 10.3390/ijms12020946

Liu, W. S., Wang, R. R., Li, W. Y., Rong, M., Liu, C. L., Ma, Y., & Wang, R. L. (2019). Investigating the reason for loss-of-function of Src homology 2 domain-containing protein tyrosine phosphatase 2 (SHP2) caused by Y279C mutation through molecular dynamics simulation. *J Biomol Struct Dyn*, 1-12. doi: 10.1080/07391102.2019.1634641

Liu, W. S., Wang, R. R., Sun, Y. Z., Li, W. Y., Li, H. L., Liu, C. L., . . . Wang, R. L. (2019).

Exploring the effect of inhibitor AKB-9778 on VE-PTP by molecular docking and molecular dynamics simulation. *J Cell Biochem*. doi: 10.1002/jcb.28963

Loeffler, H. H., & Winn, M. D. (2013). Ligand binding and dynamics of the monomeric epidermal growth factor receptor ectodomain. *Proteins*, *81*(11), 1931-1943. doi: 10.1002/prot.24339

Ma, Y., Wang, S. Q., Xu, W. R., Wang, R. L., & Chou, K. C. (2012). Design novel dual agonists for treating type-2 diabetes by targeting peroxisome proliferator-activated receptors with core hopping approach. *PLoS One*, *7*(6), e38546. doi: 10.1371/journal.pone.0038546

Machaba, K. E., Mhlongo, N. N., & Soliman, M. E. S. (2018). Induced Mutation Proves a Potential Target for TB Therapy: A Molecular Dynamics Study on LprG. *Cell Biochem Biophys*, *76*(3), 345-356. doi: 10.1007/s12013-018-0852-7

Maisuradze, G. G., Liwo, A., & Scheraga, H. A. (2009). Principal component analysis for protein folding dynamics. *J Mol Biol*, *385*(1), 312-329. doi: 10.1016/j.jmb.2008.10.018

Miyake, M., Koga, T., Kondo, S., Yoda, N., Emoto, C., Mukai, T., & Toguchi, H. (2017). Prediction of drug intestinal absorption in human using the Ussing chamber system: A comparison of intestinal tissues from animals and humans. *Eur J Pharm Sci*, *96*, 373-380. doi: 10.1016/j.ejps.2016.10.006

Ndagi, U., Mhlongo, N. N., & Soliman, M. E. (2017). The impact of Thr91 mutation on c-Src resistance to UM-164: molecular dynamics study revealed a new opportunity for drug design. *Mol Biosyst*, *13*(6), 1157-1171. doi: 10.1039/c6mb00848h

- Ndagi, U., Mhlongo, N. N., & Soliman, M. E. (2018). Emergence of a Promising Lead Compound in the Treatment of Triple Negative Breast Cancer: An Insight into Conformational Features and Ligand Binding Landscape of c-Src Protein with UM-164. *Appl Biochem Biotechnol*, *185*(3), 655-675. doi: 10.1007/s12010-017-2677-z
- Neves, B. J., Braga, R. C., Melo-Filho, C. C., Moreira-Filho, J. T., Muratov, E. N., & Andrade, C. H. (2018). QSAR-Based Virtual Screening: Advances and Applications in Drug Discovery. *Front Pharmacol*, *9*, 1275. doi: 10.3389/fphar.2018.01275
- Olde Scheper, T. V., Meredith, R. M., Mansvelder, H. D., van Pelt, J., & van Ooyen, A. (2017). Dynamic Hebbian Cross-Correlation Learning Resolves the Spike Timing Dependent Plasticity Conundrum. *Front Comput Neurosci*, *11*, 119. doi: 10.3389/fncom.2017.00119
- Pol-Fachin, L., Fernandes, C. L., & Verli, H. (2009). GROMOS96 43a1 performance on the characterization of glycoprotein conformational ensembles through molecular dynamics simulations. *Carbohydr Res*, *344*(4), 491-500. doi: 10.1016/j.carres.2008.12.025
- Schneider, G., & Fechner, U. (2005). Computer-based de novo design of drug-like molecules. *Nat Rev Drug Discov*, *4*(8), 649-663. doi: 10.1038/nrd1799
- Su, J., Liu, X., Zhang, S., Yan, F., Zhang, Q., & Chen, J. (2018). A computational insight into binding modes of inhibitors XD29, XD35, and XD28 to bromodomain-containing protein 4 based on molecular dynamics simulations. *J Biomol Struct Dyn*, *36*(5), 1212-1224. doi: 10.1080/07391102.2017.1317666
- Sun, W., Zhang, B., Zheng, H., Zhuang, C., Li, X., Lu, X., . . . Xiu, Z. (2017). Trivaric acid, a

new inhibitor of PTP1b with potent beneficial effect on diabetes. *Life Sci*, 169, 52-64.

doi: 10.1016/j.lfs.2016.11.012

Sun, W., Zhuang, C., Li, X., Zhang, B., Lu, X., Zheng, Z., & Dong, Y. (2017). Varic acid analogues from fungus as PTP1B inhibitors: Biological evaluation and structure-activity relationships. *Bioorg Med Chem Lett*, 27(15), 3382-3385. doi: 10.1016/j.bmcl.2017.06.001

Susnow, R. G., & Dixon, S. L. (2003). Use of robust classification techniques for the prediction of human cytochrome P450 2D6 inhibition. *J Chem Inf Comput Sci*, 43(4), 1308-1315. doi: 10.1021/ci030283p

Tadic, M., & Cuspidi, C. (2015). Type 2 diabetes mellitus and atrial fibrillation: From mechanisms to clinical practice. *Arch Cardiovasc Dis*, 108(4), 269-276. doi: 10.1016/j.acvd.2015.01.009

Tang, J., Qu, Z., Luo, J., He, L., Wang, P., Zhang, P., . . . Huang, Y. (2018). Molecular Dynamics Simulations of the Oil-Detachment from the Hydroxylated Silica Surface: Effects of Surfactants, Electrostatic Interactions, and Water Flows on the Water Molecular Channel Formation. *J Phys Chem B*, 122(6), 1905-1918. doi: 10.1021/acs.jpcc.7b09716

Thiyagarajan, V., Lin, S. H., Chang, Y. C., & Weng, C. F. (2016). Identification of novel FAK and S6K1 dual inhibitors from natural compounds via ADMET screening and molecular docking. *Biomed Pharmacother*, 80, 52-62. doi: 10.1016/j.biopha.2016.02.020

Wan, H., Hu, J. P., Tian, X. H., & Chang, S. (2013). Molecular dynamics simulations of wild

- type and mutants of human complement receptor 2 complexed with C3d. *Phys Chem Chem Phys*, *15*(4), 1241-1251. doi: 10.1039/c2cp41388d
- Wang, M. Y., Jin, Y. Y., Wei, H. Y., Zhang, L. S., Sun, S. X., Chen, X. B., . . . Wang, R. L. (2015). Synthesis, biological evaluation and 3D-QSAR studies of imidazolidine-2,4-dione derivatives as novel protein tyrosine phosphatase 1B inhibitors. *Eur J Med Chem*, *103*, 91-104. doi: 10.1016/j.ejmech.2015.08.037
- Wesson, L., & Eisenberg, D. (1992). Atomic solvation parameters applied to molecular dynamics of proteins in solution. *Protein Sci*, *1*(2), 227-235. doi: 10.1002/pro.5560010204
- Xu, L., Kong, R., Zhu, J., Sun, H., & Chang, S. (2016). Unraveling the conformational determinants of LARP7 and 7SK small nuclear RNA by theoretical approaches. *Mol Biosyst*, *12*(8), 2613-2621. doi: 10.1039/c6mb00252h
- Yan, F., Liu, X., Zhang, S., Su, J., Zhang, Q., & Chen, J. (2019). Electrostatic interaction-mediated conformational changes of adipocyte fatty acid binding protein probed by molecular dynamics simulation. *J Biomol Struct Dyn*, *37*(14), 3583-3595. doi: 10.1080/07391102.2018.1520648
- Yesudhas, D., Anwar, M. A., Panneerselvam, S., Durai, P., Shah, M., & Choi, S. (2016). Structural Mechanism behind Distinct Efficiency of Oct4/Sox2 Proteins in Differentially Spaced DNA Complexes. *PLoS One*, *11*(1), e0147240. doi: 10.1371/journal.pone.0147240
- Zabolotny, J. M., Bence-Hanulec, K. K., Stricker-Krongrad, A., Haj, F., Wang, Y., Minokoshi, Y., . . . Neel, B. G. (2002). PTP1B regulates leptin signal transduction in vivo. *Dev Cell*,

2(4), 489-495.

Zhai, M., Liu, S., Gao, M., Wang, L., Sun, J., Du, J., . . . Zhang, W. (2019).

3,5-Diaryl-1H-pyrazolo[3,4-b]pyridines as potent tubulin polymerization inhibitors:

Rational design, synthesis and biological evaluation. *Eur J Med Chem*, 168, 426-435.

doi: 10.1016/j.ejmech.2018.12.053

Zhang, J., Luan, C. H., Chou, K. C., & Johnson, G. V. (2002). Identification of the N-terminal

functional domains of Cdk5 by molecular truncation and computer modeling. *Proteins*,

48(3), 447-453. doi: 10.1002/prot.10173

Zhou, Y., Zhang, N., Chen, W., Zhao, L., & Zhong, R. (2016). Underlying mechanisms of cyclic

peptide inhibitors interrupting the interaction of CK2alpha/CK2beta: comparative

molecular dynamics simulation studies. *Phys Chem Chem Phys*, 18(13), 9202-9210.

doi: 10.1039/c5cp06276d

Accepted Manuscript